5050 *Chem. Mater.* **2009,** *21,* 5050–5057
DOI:10.1021/cm9014496

CHEMISTRY OF MATERIALS
Article

Enhanced Magnetization and Modulated Orbital Hybridization in Epitaxially Constrained $BiFeO_3$ Thin Films with Rhombohedral Symmetry

Sangwoo Ryu,[†] Jae-Young Kim,[‡] Young-Han Shin,[†] Byeong-Gyu Park,[‡] Jong Yeog Son,[†] and Hyun Myung Jang*,[†]

[†]*Department of Materials Science and Engineering and Division of Advanced Materials Science and,* [‡]*Pohang Accelerator Laboratory, Pohang University of Science and Technology (POSTECH), Pohang 790-784, Republic of Korea*

Received May 27, 2009. Revised Manuscript Received September 7, 2009

$BiFeO_3$ (BFO) is currently considered to be the most promising candidate material for device applications of room-temperature multiferroics. However, there exist some controversial arguments on the origin of the enhanced magnetization and polarization observed in the epitaxially constrained BFO thin film heterostructures. More specifically, the issue can be addressed by the following question: Can the epitaxial strain enhance the magnetization and the ferroelectric polarization in BFO? To clarify this controversial issue, we have systematically examined the magnetization characteristics of the rhombohedral BFO films epitaxially grown on (111)-oriented $SrTiO_3$ (STO) in terms of the in-plane misfit strain between the BFO layer and the STO substrate. The increase in the saturation magnetization with decreasing film thickness was found to be closely related with the misfit strain. By carefully examining synchrotron X-ray absorption spectra, we have further correlated the enhanced magnetization in a highly strained film with the reduced degree of hybridization between Fe 3d and O 2p orbitals and with the splitting of the triplet t_{2g} orbital into a_{1g} and e_g^{π} orbitals arising from the trigonal D_{3d} distortion.

1. Introduction

Multiferroics combine two or more of the properties of ferromagnetism (or antiferromagnetism), ferroelectricity, and ferroelasticity.[1] Under an external magnetic field, such materials would show induced electric polarization, whereas an external electric field would induce magnetization. Multiferroism is currently the subject of intensive scientific investigation[2−9] because these materials not only exhibit fascinating physical properties but also potentially offer a wide range of new applications.[1,2,5,7,8]

Unlike Mn-based oxide multiferroics such as $TbMnO_3$,[3] $TbMn_2O_5$,[4] $HoMnO_3$,[5] $YMnO_3$,[10] and $BiMnO_3$,[11] $BiFeO_3$ (BFO) exhibits room-temperature multiferroism with its ferroelectric T_C at ∼1103 K and antiferromagnetic T_N at ∼643 K.[12] Because of a residual moment from canted spin structure, BFO is actually characterized by a weak ferromagnetism at room temperature.[12] Because the room-temperature multiferroism is essential to the realization of multiferroic devices that exploit the coupling between ferroelectric and ferromagnetic orders at ambient conditions, BFO, together with more recently revealed $LuFe_2O_4$,[6,13−15] are currently considered to be promising candidates for practical device applications.[16]

The recent boom in multiferroic thin films was indeed triggered by the work of Wang et al.[2] on the enhancement of remanent polarization (P_r) and saturation magnetization

*To whom correspondence should be addressed. E-mail: hmjang@postech.ac.kr.

(1) Hill, N. A. *J. Phys. Chem. B* **2000**, *104*, 6694–6709.
(2) Wang, J.; Neaton, J. B.; Zheng, H.; Nagarajan, V.; Ogale, S. B.; Liu, B.; Viehland, D.; Vaithyanathan, V.; Schlom, D. G.; Waghmare, U. V.; Spaldin, N. A.; Rabe, K. M.; Wuttig, M.; Ramesh, R. *Science* **2003**, *299*, 1719–1722.
(3) Kimura, T.; Goto, T.; Shintani, H.; Ishizaka, K.; Arima, T.; Tokura, Y. *Nature* **2003**, *426*, 55–58.
(4) Hur, N.; Park, S.; Sharma, P. A.; Ahn, J. S.; Guha, S.; Cheong, S. W. *Nature* **2004**, *429*, 392–395.
(5) Lottermoser, T.; Lonkai, T.; Amann, U.; Hohlwein, D.; Ihringer, J.; Fiebig, M. *Nature* **2004**, *430*, 541–544.
(6) Ikeda, N.; Ohsumi, H.; Ohwada, K.; Ishii, K.; Inami, T.; Kakurai, K.; Murakami, Y.; Yoshii, K.; Mori, S.; Horibe, Y.; Kito, H. *Nature* **2005**, *436*, 1136–1138.
(7) Eerenstein, W.; Mathur, N. D.; Scott, J. F. *Nature* **2006**, *442*, 759–765.
(8) Zhao, T.; Scholl, A.; Zavaliche, F.; Lee, K.; Barry, M.; Doran, A.; Cruz, M. P.; Chu, Y. H.; Ederer, C.; Spaldin, N. A.; Das, R. R.; Kim, D. M.; Baek, S. H.; Eom, C. B.; Ramesh, R. *Nat. Mater.* **2006**, *5*, 823–829.
(9) Ishiwata, S.; Taguchi, Y.; Murakawa, H.; Onose, Y.; Tokura, Y. *Science* **2008**, *319*, 1643–1646.
(10) Huang, Z. J.; Cao, Y.; Sun, Y. Y.; Xue, Y. Y.; Chu, C. W. *Phys. Rev. B* **1997**, *56*, 2623–2626.
(11) Hill, N. A.; Rabe, K. M. *Phys. Rev. B* **1999**, *59*, 8759–8769. Santos, A. M.; Parashar, S.; Raju, A. R.; Zhao, Y. S.; Cheetham, A. K.; Rao, C. N. R. *Solid State Commun.* **2002**, *122*, 49–52.
(12) Ederer, C.; Spaldin, N. A. *Phys. Rev. B* **2005**, *71*, 060401.
(13) Subramanian, M. A.; He, T.; Chen, J.; Rogado, N. S.; Calvarese, T. G.; Sleight, A. W. *Adv. Mater.* **2006**, *18*, 1737–1739.
(14) Xiang, H. J.; Whangbo, M.-H. *Phys. Rev. Lett.* **2007**, *98*, 246403.
(15) Park, J. Y.; Park, J. H.; Jeong, Y. K.; Jang, H. M. *Appl. Phys. Lett.* **2007**, *91*, 152903.
(16) Martin, L. W.; Chu, Y.-H.; Holcomb, M. B.; Huijben, M.; Yu, P.; Han, S.-J.; Lee, D.; Wang, S. X.; Ramesh, R. *Nano Lett.* **2008**, *8*(7), 2050–2055.

 Published on Web 10/07/2009

(M_s) in the epitaxially constrained BFO heterostructures. More specifically, they reported that the [001]-oriented epitaxially constrained BFO thin film with pseudotetragonal symmetry exhibited dramatically enhanced P_r ($\sim$60 μCoul/cm^2) and M_s ($\sim$150 emu/cm^3). Here, P_r defines the polarization value at an applied electric field of zero in a saturated polarization-field ($P-E$) hysteresis curve, whereas M_s denotes a saturated value of the magnetization in a given magnetization-field ($M-H$) curve. Wang and co-workers[2] attributed these enhanced P_r and M_s values to a strong compressive in-plane stress imposed by the bottom $SrRuO_3/SrTiO_3$ (SRO/STO) structure. However, a group of scientists at Cambridge[17] argued that the epitaxial misfit strain did not enhance the ferromagnetic and ferroelectric properties of heteroepitaxially grown BFO films. Instead, they insisted that the coexistence of Fe^{2+} with Fe^{3+} was primarily responsible for the observed enhancement of the film magnetization.[17] In response to the criticism raised by the Cambridge group,[17] Wang et al.[18] admitted the coexistence of Fe^{2+} with Fe^{3+} in their films but suggested a possibility of a gradual increase in the spin canting angle with decreasing film thickness and thus with epitaxial strain.

For further scientific understanding and technological progresses in BFO-based multiferroic films, it is thus highly important to clarify the role of the in-plane misfit strain on the variations of M_s and P_r. However, both groups[2,17] examined the variations of M_s and P_r as a function of the film thickness rather than in terms of the misfit strain. To resolve this critical issue, one has to thus carefully examine magnetic and ferroelectric properties as a function of the misfit strain. Here we report the effect of the in-plane misfit strain on the magnetic response of the rhombohedral BFO films epitaxially grown along the principal polarization direction.[19] We have shown that M_s of the film is directly related to the magnitude of the in-plane misfit strain. We have further correlated the enhanced magnetization in a highly strained film with the reduced degree of the hybridization between Fe3d and O2p orbitals.

2. Experimental Methods

BFO thin films with their out-of-plane direction parallel to the pseudocubic $[111]_c$ direction (or equivalently parallel to hexagonal $[001]_h$ direction) were grown on STO (111) substrates by employing pulsed laser deposition (PLD) method.[20] KrF excimer laser with the wavelength of 248 nm was used for this purpose. The deposition was carried out at 675 °C under P_{O_2} = 10 mTorr. In the preparation of a ceramic BFO target, a slightly excess amount of bismuth was used to compensate its high volatility at the deposition temperature.

For the structural characterizations of the BFO thin films, both high-resolution X-ray diffraction (HR-XRD) pattern and reciprocal space mapping (RSM) were obtained by utilizing a D8 Discover X-ray diffractometer by Bruker AXS with the combination of a Göbel mirror for primary optics and a Ge(220) triple bounce analyzer crystal for secondary optics. A JEM-2100F Cs-corrected HR-STEM (high-resolution scanning transmission electron microscope) operating at 200 kV by JEOL and an ESCALAB 220iXL with Mg Kα by VG Scientific were, respectively, used for TEM and XPS (X-ray photoelectron spectroscopy) analysis.

Magnetization responses of the BFO films were examined by measuring magnetization-field (M-H) hysteresis curves using a superconducting quantum interference device (SQUID) magnetometer (MPMS-5S; Quantum Design). The magnetic field was applied along the in-plane direction (i.e., perpendicular to $[111]_c$ or $[001]_h$), which is known to be the magnetic easy axis.[21] To examine anisotropy in the film magnetization, we also measured $M-H$ curves with the applied magnetic field parallel to the out-of-plane direction.

To investigate the origin of the evolution of the magnetic properties, hard X-ray absorption near edge structure (XANES) at Fe *K*-edge experiment was carried out at 7C1 XAFS II beamline, and soft X-ray absorption spectroscopy (XAS) measurements at O *K*-edge and Fe $L_{2,3}$-edge were carried out at 2A MS beamline of Pohang Light Source (PLS). While the fluorescence mode was used for XANES, the total electron yield mode was employed for both Fe $L_{2,3}$-edge XAS and polarization-dependent O *K*-edge XAS. In the polarization-dependent XAS experiment, an elliptically polarized undulator (EPU) was inserted at 2A beamline so that the beam polarization could be properly adjusted without rotating the sample specimen. This enabled us to obtain more accurate XAS data. We reduced the beam flux to a sufficiently low level and carried out the XAS measurement at an elevated temperature of 350 K to minimize possible charging effect on the peak intensity. Actually, we observed no polarization-dependent beam flux in our measurements, suggesting that a charging effect was minimized.

We have normalized *O* K-edge XAS spectra using the spectral intensity at the region above 560 eV, which corresponds to a continuum spectral state and is thus proportional to the number of the core 1s electrons of oxygen atom. By equalizing the intensity at the region above 560 eV, we were able to obtain the spectral intensity which is proportional to a single oxygen atom. Regarding the spectral resolution, 0.05 eV which corresponds to the estimated $a_{1g}-e_g^{\pi}$ splitting (see the Results and Discussion section) is safely within the resolution limit of PLS.

3. Results and Discussion

Thickness-Dependent In-Plane Misfit Strain. Figure 1a presents a narrow section of the $\theta-2\theta$ X-ray diffraction ($\theta-2\theta$ XRD) patterns of the $[111]_c$-oriented BFO films grown on STO (111) around their (111) pseudocubic reflections. Similarly, Figure 1b shows the XRD patterns around their (002) reflections. It is clear from these XRD results that the out-of-plane lattice parameter of BFO depends on the film thickness and that d_{111}(BFO) > d_{111}(STO) for all four BFO films grown on STO (111). It is interesting to note that the $(002)_c$ diffraction peak

(17) Eerenstein, W.; Morrison, F. D.; Dho, J.; Blamire, M. G.; Scott, J. F.; Mathur, N. D. *Science* **2005**, *307*, 1203a.
(18) Wang, J.; Scholl, A.; Zheng, H.; Ogale, S. B.; Viehland, D.; Schlom, D. G.; Spaldin, N. A.; Rabe, K. M.; Wuttig, M.; Mohaddes, L.; Neaton, J.; Waghmare, U.; Zhao, T.; Ramesh, R. *Science* **2005**, *307*, 1203b.
(19) Selbach, S. M.; Tybell, T.; Einarsrud, M.-A.; Grande, T. *Chem. Mater.* **2007**, *19*, 6478–6484.
(20) Singh, M. K.; Jang, H. M.; Ryu, S.; Jo, M.-H. *Appl. Phys. Lett.* **2006**, *88*, 042907.
(21) Ruette, B.; Zvyagin, S.; Pyatakov, A. P.; Bush, A.; Li, J. F.; Belotelov, V. I.; Zvezdin, A. K.; Viehland, D. *Phys. Rev. B* **2004**, *69*, 064114.

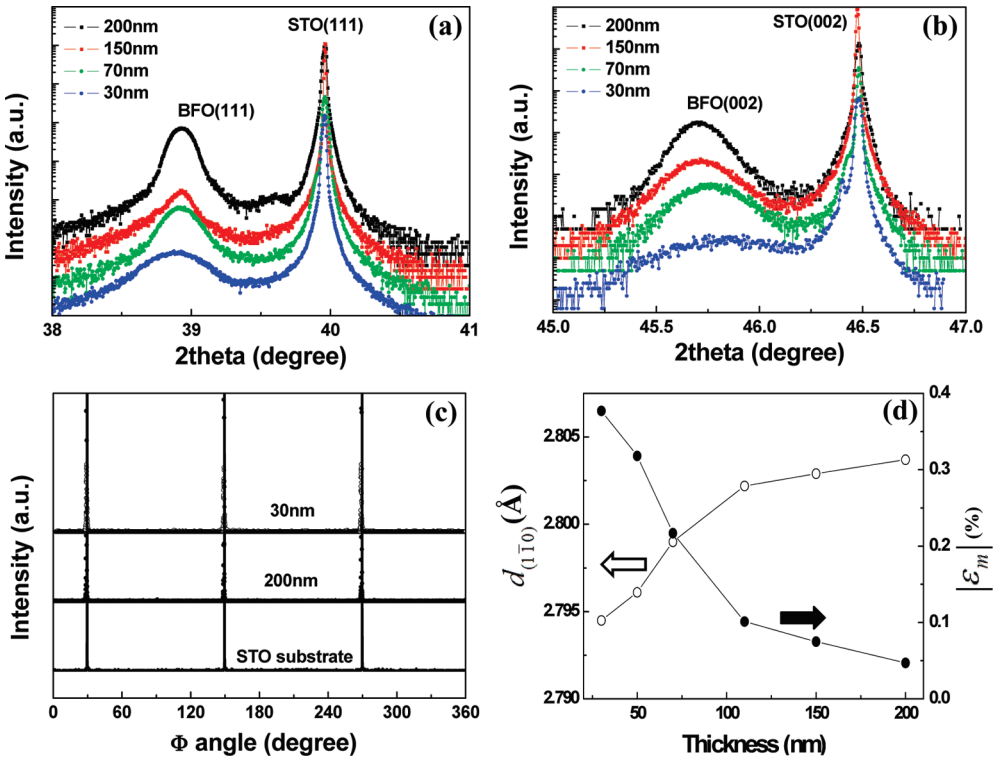

Figure 1. $\theta-2\theta$ XRD patterns of four different BFO thin films around their (a) (111) reflections and (b) (002) reflections. (c) XRD Φ-scan diffraction patterns of STO substrate and BFO films at two different thicknesses. (d) The thickness-dependent in-plane misfit strain (filled circles) and the corresponding $d_{(1\bar{1}0)c}$ (open circles) for six epitaxial BFO thin films with different thicknesses.

shifts to a higher angle while the $(111)_c$ peak moves slightly toward a lower angle with decreasing film thickness. These results clearly indicate that all the $[111]_c$-oriented films are compressively strained by the STO substrate along the in-plane direction. The degree of the in-plane orientation was assessed by examining Φ-scan spectra. These revealed the 3-fold *R*3*c* symmetry about the $[111]_c$ direction and a coherent, so-called "cube-on-cube" epitaxial growth of BFO films on STO (111) substrates as shown in Figure 1c.

The *d*-spacing values of $(111)_c$ and $(001)_c$ planes were evaluated for six different film thicknesses, and the in-plane pseudocubic parameter $d_{(1\bar{1}0)c}$ was estimated using the relation: $d_{(1\bar{1}0)c} = d_{(001)c}/\sqrt{2}$. The misfit strain ($|\varepsilon_m|$) was then calculated using the following relation: $\varepsilon_m = (a_{eff} - a_{free})/a_{eff}$, where a_{eff} is the effective in-plane lattice parameter of the constrained film ($= d_{(1\bar{1}0)c}$) and a_{free} is that of the stress-free state. Thus, a_{free} is equal to $a/\sqrt{2}$ where *a* is the unstrained pseudocubic lattice parameter ($= 3.965$ Å[22]). The calculated in-plane lattice parameter and the corresponding misfit strain are presented in Figure 1d as a function of the film thickness.

Evidence of the relaxation of the in-plane misfit strain was obtained by performing RSM experiments. The intensity contours around (021) reflection were collected for three epitaxially grown films with different thicknesses. [111] and [-110] directions were, respectively, set as the surface normal and azimuthal axes. After collecting the diffraction patterns in the $2\theta-\omega$ space with the step size of 0.01 and 0.005° for 2θ and ω, respectively, we have converted the $2\theta-\omega$ space map into the q_x-q_z space map by using Leptos software from Bruker AXS. Figure 2 presents the RSM data around (021) reflection of 30, 70, and 200-nm-thick BFO films preferentially grown along $[111]_c$. The contours tend to be broad because a large slit optic was used to produce a sufficient intensity, instead of an analyzer crystal. As presented in Figure 2, the reciprocal scattering vector along $(\bar{1}10)$ (i.e., q_x) of all three films is different from that of the substrate, STO (111). This indicates that the film is partially relaxed at a thickness as thin as 30 nm. As shown in Figure 2, the difference in q_x between the film and the substrate increases with the film thickness, which suggests a gradual relaxation of the in-plane misfit strain with the thickness. More specifically, we have the following values of the thickness-dependent in-plane misfit strain: (i) 0.377% for 30 nm, (ii) 0.217% for 70 nm, and (iii) 0.047% for 200 nm. Compared with the BFO film grown on a STO (001) substrate, in which the ferroic layer with the pseudotetragonal symmetry is highly strained up to ~80 nm,[23] the present film with the *R*3*c* symmetry is partially relaxed even at 30 nm. These observations can be attributed to the difference in the relaxation mechanism of the elastic energy between these two different crystalline states.[24]

(22) Chu, Y.-H.; Zhan, Q.; Martin, L. W.; Cruz, M. P.; Yang, P.-L.; Pabst, G. W.; Zavaliche, F.; Yang, S.-Y.; Zhang, J.-X.; Chen, L.-Q.; Schlom, D. G.; Lin, I.-N.; Wu, T.-B.; Ramesh, R. *Adv. Mater.* **2006**, *18*, 2307–2311.

(23) Béa, H.; Bibes, M.; Petit, S.; Kreisel, J.; Barthélémy, A. *Philos. Mag. Lett.* **2007**, *87*, 165–174.

(24) Béa, H.; Bibes, M.; Zhu, X.-H.; Fusil, S.; Bouzehouane, K.; Petit, S.; Kreisel, J.; Barthélémy, A. *Appl. Phys. Lett.* **2008**, *93*, 072901.

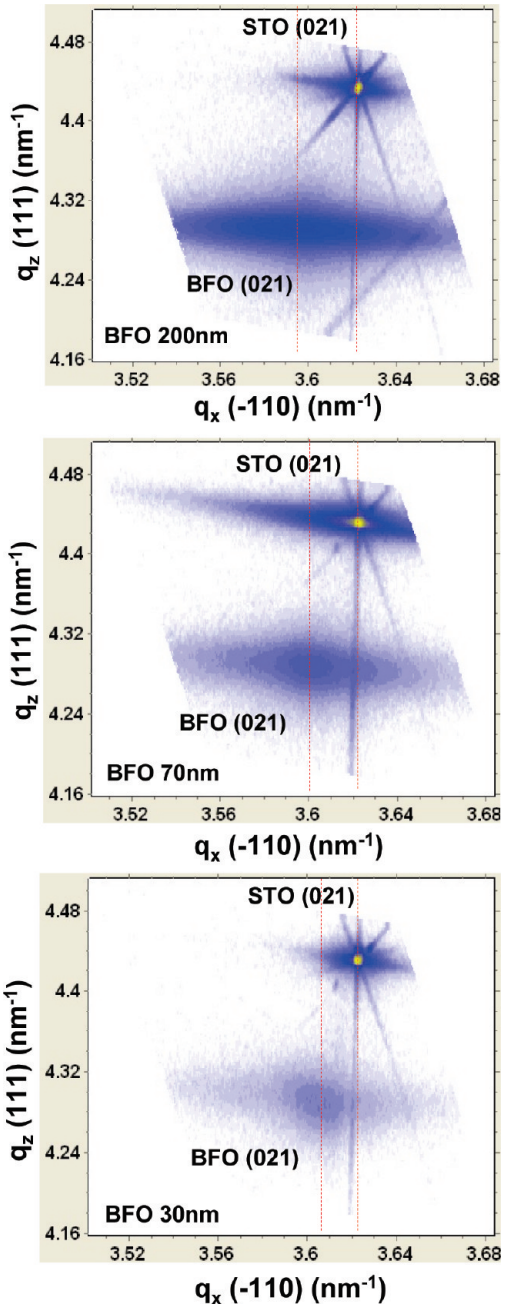

Figure 2. RSM data around the (021) reflection of the 30, 70, and 200-nm-thick epitaxial BFO films in the $q_x(\bar{1}10) - q_z(111)$ space.

Transmission Electron Microscopy and X-ray Absorption Spectroscopy. A cross-sectional HR-TEM image of the 30-nm-thick BFO film (Figure 3a) shows continuous and straight atomic lines along [110] and [001] directions through the interface, which indicates that the film is grown heteroepitaxially. As presented in Figure 3b, the inverse Fourier-transformed image obtained using the electron diffraction pattern (inset of Figure 3a) more clearly demonstrates the epitaxial growth. We have further carefully examined a possible presence of an interfacial impurity layer or precipitates in our BFO films by HR-STEM analysis. However, HR-STEM study indicates that there is no impurity phase at the interfacial region, as revealed in Figure 3c.

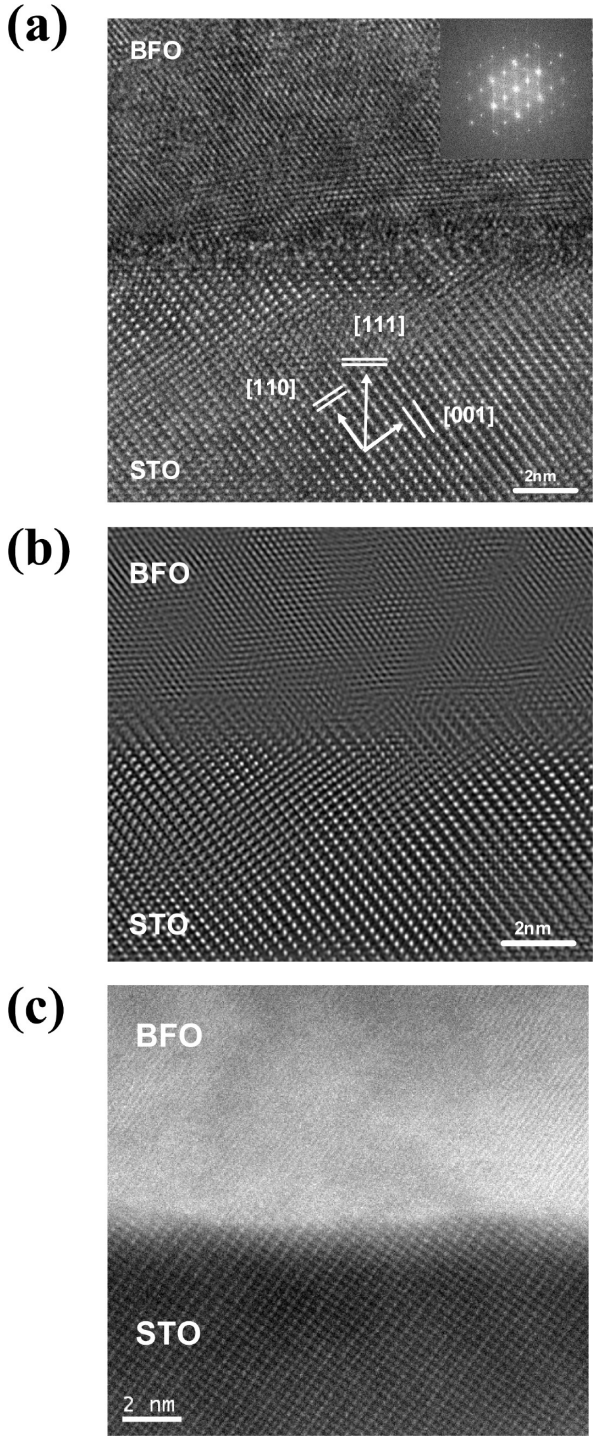

Figure 3. Cross-sectional HR-TEM images of the 30-nm-thick BFO film epitaxially grown on STO (111): (a) a HR-TEM image around [1$\bar{1}$0] zone with an electron diffraction pattern (inset), and (b) an inverse Fourier transformed image. (c) HR-STEM HAADF (high angle annular dark field) image of the 30 nm thick BFO film.

To clearly isolate the effect of the in-plane misfit strain on the magnetic properties, it is necessary to prepare heteroepitaxially grown BFO thin films in which divalent Fe ions are effectively removed. For this purpose, we first examined X-ray photoelectron spectra of the epitaxially grown BFO films. Considering that Fe $2p_{3/2}$ main peak

(25) Schedel-Niedrig, Th.; Weiss, W.; Schlögl, R. *Phys. Rev. B* **1995**, *52*, 17449.

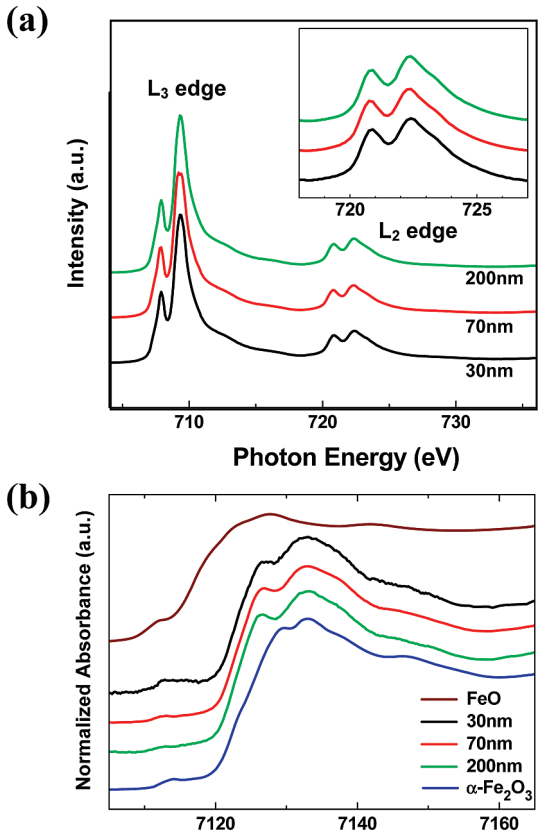

Figure 4. Room-temperature X-ray absorption spectroscopic results of the $[111]_c$-oriented epitaxial BFO thin films at three different thicknesses: (a) XAS near Fe $L_{2,3}$ edges; inset, the magnified L_2 region; and (b) XANES spectra.

occurs at 709.5 eV for Fe^{2+} and at 711.0 eV for Fe^{3+},[25] we have separated a given XPS spectrum (Fe 2p line) into two distinctive peaks. The peak-fitting result indicates that regardless of the film thickness, the fraction of Fe^{2+} is essentially negligible. Thus, it can be concluded that Fe ions in our BFO films exist as the trivalent state.

This conclusion was further inspected by examining X-ray absorption spectra (XAS) near the Fe $L_{2,3}$-edge region. It is well-known that Fe_2O_3 which consists of trivalent Fe ions exclusively exhibits doublet peaks at both L_2 and L_3 edges in its XAS spectrum. As shown in Figure 4a, the BFO films are also characterized by obvious doublet peaks at both L_2 (~709 eV) and L_3 (~722 eV) edges. In addition to this, the peak positions of our BFO films are nearly the same as those of Fe_2O_3.[26] These observations indicate that the divalent Fe ions are practically absent in our BFO films. On the contrary, the L-edge spectrum of FeO does not show any doublet peak at both L_2 and L_3 edges, with its peak position at a slightly lower photon energy than the corresponding L-edge peak position of Fe_2O_3.[26] The absence of a pre-edge peak (at ~719 eV) in front of the L_2 doublet centered at 721.5 eV (inset of Figure 4a) further supports that the divalent Fe ions are absent in our PLD-grown BFO films.

(26) Kim, G.; Lee, S. S.; Wi, S. C.; Kang, J.-S.; Han, S. W.; Kim, J. Y.; Lee, B. W.; Kim, J. Y.; Shin, H. J.; Parr, B. G.; Park, J.-H.; Min, B. I. *J. Appl. Phys.* **2006**, *99*, 08Q309.

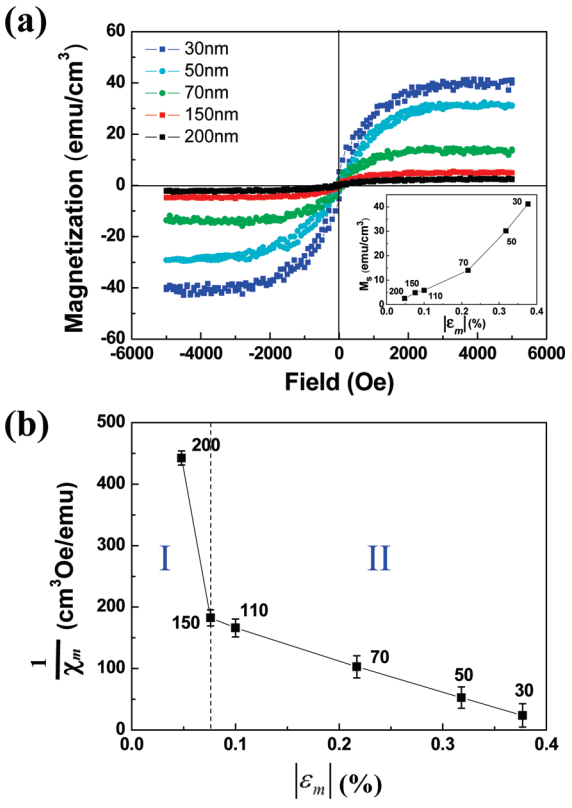

Figure 5. (a) Room-temperature magnetization-field ($M-H$) hysteresis curves of the $[111]_c$-oriented epitaxial BFO thin films grown on STO (111). The inset shows the saturation magnetization (M_s) plotted as a function of the in-plane misfit strain, $|\varepsilon_m|$ (%). (*b*) Zero-field-limit inverse magnetic susceptibility of the $[111]_c$-oriented epitaxial BFO films plotted as a function of the misfit strain, $|\varepsilon_m|$ (%). Various numerical values appeared in the vicinity of each data point denote the film thickness in nanometers (nm).

The probing depth of these two spectroscopic methods (i.e., XPS and XAS) is limited to a few nanometers from the surface. Thus, we have examined the oxidation state of Fe ions in the interior region of the film by employing XANES, in which hard X-ray beams are able to penetrate into the bulk region which is a few hundred nanometers away from the surface. We have examined the oxidation state of Fe ions in the bulk region by comparing the XANES spectra of the BFO films with those of α-Fe_2O_3 and FeO, where α-Fe_2O_3 is characterized by the same FeO_6 octahedral structure and by the trivalent Fe ions exclusively. On the other hand, FeO contains only divalent Fe ions. As presented in Figure 4b, both α-Fe_2O_3 and the BFO films exhibit similar spectral features, i.e., a doublet peak at the Fe K absorption edge (at ~7126 and 7133 eV),[27] indicating that all the Fe ions in the interior region of the films are in the trivalent state. The absence of a shoulder peak[27] at the absorption energy slightly lower than that of the doublet peak further supports the absence of divalent Fe ions in our BFO films.

Enhanced Magnetization and Modulated Orbital Hybridization. As presented in Figure 5a, all the epitaxial BFO films exhibit a weak ferromagnetic behavior under the magnetic field applied parallel to the in-plane direction

(27) Sasaki, S. *Rev. Sci. Instrum.* **1995**, *66*, 1573–1576.

(i.e., perpendicular to $[111]_c$ or $[001]_h$ [21]). One prominent feature of Figure 5a is that both the saturation magnetization (M_s) and the magnetic susceptibility (χ_m) decrease with increasing film thickness, suggesting that both M_s and χ_m depend on the misfit strain. Indeed, M_s of the epitaxially grown films correlates well with the magnitude of the misfit strain, ($|\varepsilon_m|$) (inset of Figure 5a). Having established that Fe^{2+} ions practically do not exist in all the $[111]_c$-oriented BFO films, we are now able to make a conclusion that the increase in M_s with decreasing film thickness is mainly caused by the misfit strain between the BFO film and the STO substrate. On the contrary, we observed that M_s of the BFO films under the magnetic field applied parallel to the out-of-plane direction (i.e., parallel to $[111]_c$ or $[001]_h$) was essentially independent of the film thickness with a negligibly small value of M_s. This further indicates that the canted spin moment along the in-plane direction is the source of the enhanced M_s, in response to the increase in the in-plane misfit strain.

Having obtained a macroscopic correlation of the magnetization with the misfit strain, ($|\varepsilon_m|$), we now examine a microscopic origin of the enhanced M_s with ($|\varepsilon_m|$). It can be shown that with the help of the Landau theory of ferromagnetism, the inverse magnetic susceptibility ($1/\chi_m$) of an epitaxially constrained film is proportional to ($|\varepsilon_m|$). Thus, we have plotted $1/\chi_m$ as a function of the misfit strain to see some interesting physics. As shown in Figure 5b, there appear two distinct regions in the $1/\chi_m$ vs ($|\varepsilon_m|$) plot, and the slope of region I is much more negative than that of region II. The inverse magnetic susceptibility increases rapidly as ($|\varepsilon_m|$) becomes smaller than a certain critical value (~0.08%).

According to the study of Bai et al.,[28] the epitaxial constraint induces the destruction of a spatially modulated cycloidal spin structure in bulk BFO (with a periodicity of ~600 Å), releasing a latent antiferromagnetic component locked within the cycloid. This leads to a transition from the incommensurately modulated cycloidal spin state to the homogeneous spin state. Thus, an abrupt change in the slope between region I and region II can be understood in terms of phase transition from the cycloidal spin state to the homogeneous spin state with the onset value around 150 nm (see the Supporting Information). Figure 5b suggests that the in-plane constrained epitaxial BFO film with *R*3*c* symmetry undergoes a spontaneous transition to the homogeneous spin state below this critical thickness (or above the critical value of the misfit strain). This leads to an abrupt change in the slope of the plot at ~150 nm (Figure 5b).

As shown in Figure 5b, the $1/\chi_m$ vs ($|\varepsilon_m|$) plot in region II is also characterized by a linear line with a substantially smaller value of the slope although M_s increases steadily with the misfit strain in this region (inset of Figure 5a). To obtain a microscopic picture of this steady increase of M_s in region II, we have examined polarization-dependent XAS of the two epitaxially constrained BFO films with their misfit strains belonging to region II. The normalized O K-edge XAS of 110 and 30 nm thick epitaxial films are presented in Figure 6. The two peaks around 530.1 and 531.7 eV are attributed to the O 2p hybridization with the low lying t_{2g} and high lying e_g orbital bands of Fe 3d, respectively, with the crystal-field splitting of $10Dq \approx$ 1.6 eV. Among these two, the t_{2g} peak is known to be a useful indicator for assessing the degree of the hybridization between Fe 3d and O 2p orbitals.[29] As shown in Figure 6, both e_g and t_{2g} peaks for the out-of-plane direction are enhanced with increasing film thickness: (i) the peak height for the 30-nm-thick film: $e_g = 0.82$(a.u.) and $t_{2g} = 0.38$(a.u.), (ii) the peak height for the 110-nm-thick film: $e_g = 0.91$(a.u.) and $t_{2g} = 0.41$(a.u.). Thus, the e_g peak shows a more pronounced increase of the peak intensity with the film thickness. This observation suggests that the degree of the orbital hybridization along the out-of-plane direction is suppressed with increasing misfit strain (i.e., with decreasing film thickness). This tendency of enhancing the degree of the orbital hybridization with the film thickness is consistent with the relatively strong t_{2g} peak intensity observed in a bulk BFO, as compared with that of nanoconfined particles.[30]

It is known that under the D_{3d} trigonal symmetry, the triplet t_{2g} orbital is split into a singlet a_{1g} orbital and a doublet e_g^{π} orbital.[31] A careful examination of the absorption spectra of our BFO films also suggests the splitting of t_{2g} orbital into a_{1g} and e_g^{π} orbitals (Figure 6). This indicates that the FeO_6 octahedron in the *R*3*c* BFO undergoes a structural distortion to trigonal symmetry. In our experimental beam geometry, a_{1g} orbital is enhanced by a polarized X-ray beam along the out-of-plane direction, whereas the e_g^{π} orbital is enhanced by a polarized beam along the in-plane direction. As shown in Figure 6, the peak position for the out-of-plane polarization is lower than that for the in-plane polarization. This indicates that among these two orbitals, the a_{1g} orbital corresponds to a lower lying state.[31] The degree of the $a_{1g}-e_g^{\pi}$ splitting in each spectrum was estimated using the peakfit program based on the Voigt profile. As indicated in Figure 6, the degree of the $a_{1g}-e_g^{\pi}$ splitting increases with decreasing film thickness or with increasing out-of-plane lattice parameter. This suggests that the degree of the trigonal distortion enhances with increasing out-of-plane lattice parameter, and thus with increasing in-plane misfit strain.

The degree of the orbital overlapping along the out-of-plane direction decreases with increasing lattice parameter along this direction. Thus, the XAS intensity corresponding to the a_{1g} orbital band is expected to be decreased with increasing out-of-plane lattice parameter, i.e., with decreasing film thickness. This prediction

(28) Bai, F.; Wang, J.; Wuttig, M.; Li, J.; Wang, N.; Pyatakov, A. P.; Zvezdin, A. K.; Cross, L. E.; Viehland, D. *Appl. Phys. Lett.* **2005**, *86*, 032511.

(29) Thakur, P.; Chae, K. H.; Kim, J.−Y.; Subramanian, M.; Jayavel, R.; Asokan, K. *Appl. Phys. Lett.* **2007**, *91*, 162503.

(30) Park, T.-J.; Sambasivan, S.; Fischer, D. A.; Yoon, W.-S.; Misewich, J. A.; Wong, S. S. *J. Phys. Chem. C* **2008**, *112*, 10359–10369.

(31) Kim, J.-Y.; Koo, T.-Y.; Park, J.-H. *Phys. Rev. Lett.* **2006**, *96*, 047205.

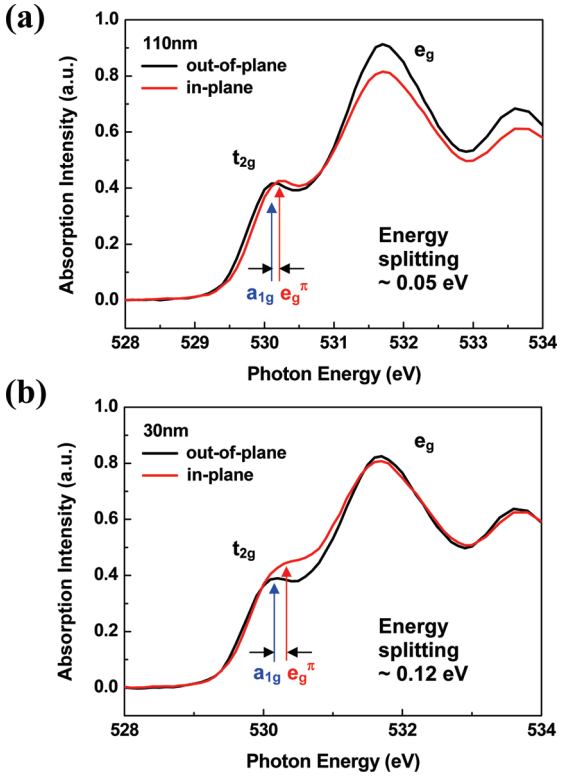

Figure 6. Polarization-dependent X-ray absorption spectra at *O* K-edge of (a) the 110-nm-thick epitaxial BFO film and (b) the 30-nm-thick epitaxial BFO film.

accounts for the observed decrease in the a_{1g} peak intensity of the 30-nm-thick, as compared with that of the 110-nm-thick. On the contrary, the peak intensity corresponding to the e_g^{π} orbital band is expected to be increased with decreasing film thickness (i.e., with decreasing in-plane lattice parameter). However, the XAS spectra presented in Figure 6 do not clearly demonstrate this prediction. This suggests a further fine splitting of the doubly degenerate e_g^{π} orbital into $e_g^{\pi}(\|)$ and $e_g^{\pi}(\perp)$ orbitals under a highly strained condition (30-nm-thick film). Because of a strong in-plane compressive strain in the 30-nm-thick film, the in-plane component of the split orbitals ($e_g^{\pi}(\|)$) now moves toward a higher energy state (i.e., toward the e_g-orbital state). This explains our observation that the degree of the $a_{1g}-e_g^{\pi}$ splitting increases with decreasing film thickness: 0.05 eV for 110 nm thick film vs 0.12 eV for 30 nm thick film (Figure 6).

The observed enhanced magnetization in a highly strained film could be correlated with a small variation of the octahedron tilt angle (θ). Considering experimental difficulty associated with measuring a subtle variation of the tilt angle in an epitaxial film (not a powder), we have theoretically computed the canted spin moment as a function of the tilt angle. For this purpose, first-principles density functional theory (DFT) calculations were carried out within the projector augmented wave method implemented in the Vienna ab initio simulation (VASP) package[32] by explicitly treating 15 valence electrons for Bi ($5d^{10}6s^26p^3$), 14 for Fe ($3p^63d^66s^24s^2$), and 6 for oxygen

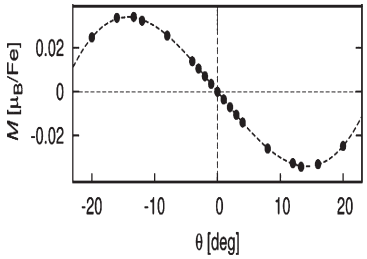

Figure 7. Computed magnetization of the rhombohedral BFO plotted as a function of the tilt angle (θ). The computed direction of M is perpendicular to $[111]_c$ which is the principal polarization direction of the *R*3*c* BFO.

($2s^22p^4$). As shown in Figure 7, the canted spin moment perpendicular to $[001]_h$ (i.e., $[111]_c$) decreases with decreasing tilt angle from its equilibrium value of 13.6°, finally ending up with $M = 0$ at $\theta = 0$. The DFT magnetization predicts that increasing tilt angle from 13.6° also reduces the computed spin moment. These computational results thus indicate that a small change in the octahedron tilt angle from its equilibrium value cannot enhance the canted spin moment along $[110]_h$ (i.e., vertical to $[111]_c$).

We have then considered other possible cause of the enhanced magnetization. The in-plane epitaxial misfit strain may cause a small distortion in the Fe−O−Fe bond angle, thus, a variation of the spin canting[33] as the weak ferromagnetic behavior of BFO is known to be manifested by the superexchange interaction through the Fe−O−Fe bond.[34] In a recent report by Prashanthi et al.,[35] the enhanced magnetization in a Dy-modified BFO was attributed to the decrease in the Fe−O−Fe bond angle. According to an interesting study done by Li and coworkers,[36] the spontaneous magnetization increases while the Fe−O−Fe bond angle decreases with decreasing content of calcium in $Nd_{1-x}Ca_xFeO_3$ orthoferrites: 6-fold increase in the spontaneous magnetization accompanied with the decrease in the Fe−O−Fe bond angle by 6° for the variation of x value from 0.5 to 0.1. In our BFO films, we observed 8-fold increase in M_s with decreasing film thickness from 150 to 30 nm (region II; Figure 5). This suggests that the Fe−O−Fe bond angle decreases (presumably less than 10°) with increasing misfit strain in region II of Figure 5b. Considering all of these, one can now deduce that the reduced degree of the orbital hybridization in a highly strained film is closely related with the observed enhanced magnetization through a small variation in the Fe−O−Fe spin canting. This results in the enhancement of the in-plane component of M_s in a highly constrained BFO film having *R*3*c* symmetry.

4. Conclusions

It was shown that the observed increase in M_s with decreasing film thickness was closely correlated with the

(32) Kresse, G.; Joubert, D. *Phys. Rev. B* **1999**, *59*, 1758–1775.
(33) Kumar, A.; Rivera, L.; Katiyar, R. S.; Scott, J. F. *Appl. Phys. Lett.* **2008**, *92*, 132913.
(34) Baettig, P.; Ederer, C.; Spaldin, N. A. *Phys. Rev. B* **2005**, *72*, 214105.
(35) Prashanthi, K.; Chalke, B. A.; Barick, K. C.; Das, A.; Dhiman, I.; Palkar, V. R. *Solid State Commun.* **2009**, *149*, 188–191.
(36) Li, J.; Kou, X.; Qin, Y.; He, H. *J. Appl. Phys.* **2002**, *92*, 7504–7509.

in-plane misfit strain between the epitaxial BFO layer and the substrate. For a small value of the misfit strain (region I), the observed increase in M_s with $|\varepsilon_m|$ (i.e., a rapid decrease in $1/\chi_m$ with $|\varepsilon_m|$) was attributed to a transition from the modulated cycloidal spin state to the homogeneous spin state. On the other hand, a further steady increase in M_s beyond this transition point (region II) was correlated with the reduced Fe3d−O2p orbital hybridization with increasing $|\varepsilon_m|$. We have further shown that the splitting of the triplet t_{2g} orbital into a_{1g} and e_g^{π} orbitals that arises from the trigonal D_{3d} distortion increases with the in-plane misfit strain.

Acknowledgment. The authors gratefully acknowledge Dr. Ju Hyung Suh at National Center for Nanomaterials Technology (NCNT), Pohang, Korea, for his assistance in our HR-STEM analysis. All the x-ray spectroscopic measurements were carried out at the Pohang Light Source (PLS) of Pohang Accelerator Laboratory, POSTECH. This work was supported by the POSTECH Basic Science Research Institute (BSRI) 2008 Grant and by the WCU program of MEST (Grant R31-2008-000-10059-0). Experimental works at PLS were supported by the Korea Research Foundation Grant funded by the Korean Government (MOEHRD, Basic Research Promotion Fund) under Contract KRF-2008-314-C00094.

Supporting Information Available: Discussion on "the transition from a spatially modulated spin state to a homogeneous spin state" (PDF). This material is available free of charge via the Internet at http://pubs.acs.org.